Author version: *Chem. Geol., vol.312-313; 2012; 127-137*

Distribution of REEs and yttrium among major geochemical phases of marine Fe-Mn-oxides: Comparative study between hydrogenous and hydrothermal deposits

L. Surya Prakash[a], Durbar Ray[a*], Anil L. Paropkari[a], Abhay V. Mudholkar[a], M. Satyanarayanan[b], B. Sreenivas[b], D. Chandrasekharam[c], Dalayya Kota[a], K. A. Kamesh Raju[a], Sujata Kaisary[a], V. Balaram[b], Tripti Gurav[c]

[a]*CSIR - National Institute of Oceanography, Dona Paula, Goa-403004, India*
[b]*CSIR - National Geophysical Research Institute, Uppal Road, Hyderabad-500007, India*
[c]*Indian Institute of Technology, Powai, Mumbai-400076, India*

Abstract

Mineralogy and geochemistry of the ferromanganese oxides collected from two seamounts in the Andaman Sea have been investigated with special reference to the solid phase partitioning behavior of rare earth elements (REEs). Bulk elemental compositions indicate that the oxides from a volcanic cratered seamount, CSM, are hydrothermal while those from another seamount, SM2, are hydrogenous in origin. The distributions of REEs and yttrium in four geochemical phases (viz. easily exchangeable, Mn-oxide, Fe-oxyhydroxide and residual) of CSM-oxides were distinctly different from that of SM2-oxides. In CSM-oxides, the REEs and yttrium are mainly associated with Fe-oxyhydroxide phase while in SM2-oxides, both Mn-oxide and Fe-oxyhydroxide phases contain the major fraction of these elements. The exchangeable and residual phases of both hydrothermal and hydrogenous oxides have extremely low REE-content. The shale normalized negative Ce-anomalies and relative enrichment of heavy REE, characteristic of hydrothermal oxides, are retained in Fe-oxyhydroxide phase. In hydrogenous oxides, the positive Ce-anomalies occurred in both Fe and Mn-oxide phases while negative Y-anomalies were found only in Fe-oxyhydroxide phase. The phase distribution of REEs and yttrium in hydrothermal oxides is described in terms of co-precipitation and adsorption of their halide complexes and available free ions in hydrothermal solutions. Instead, adsorption of major carbonate species from seawater primarily regulates the partitioning of REEs among the co-existing phases of hydrogenous oxides.

Keywords: Ferromanganese oxide, Hydrothermal, Hydrogenous, Yttrium, Rare earth elements, Elemental speciation.

***Corresponding author**

Durbar Ray
Chemical Oceanography Division,
National Institute of Oceanography, Dona Paula, Goa - 403004, India
Tel.: 91-832-2450531; Fax: 91-832-2450609; E-mail: dray@nio.org

1. Introduction

Marine ferromanganese oxides from different parts of the world oceans have been studied extensively (Calvert and Cronan, 1978; Friedrich and Schmitz-wiechowski, 1980; Elderfield et al., 1981; Aplin and Cronan, 1985; Nath et al., 1992; Hein et al., 1997; Mills et al., 2001; Koschinsky and Hein, 2003; Rajani et al., 2005). These oxides are classified as hydrothermal, hydrogenous and of mixed origin (Glasby, 2000; Mills et al., 2001). Ferromanganese oxides of different genetic origins are characterized by distinctive composition of trace and rare earth elements (REEs) (German et al., 1990; Byrne and Kim 1990; Rudnicki and Elderfield, 1992). Several factors such as the rate of precipitation, nature of geochemical components in oxides (e.g. Mn-oxides, Fe-oxyhydroxides and detrital minerals), speciation of elements in seawater and hydrothermal fluid are mainly responsible for such compositional variations (Moorby and Cronan, 1981; Koschinsky and Halbach, 1995; Bau et al., 1996; Koschinsky and Hein, 2003; Takahashi et al., 2007).

Several previous studies discussed the processes of incorporation of trace elements into marine particles particularly inorganic oxides (Glassby 1973; Elderfield et al., 1981; German et al., 1990). Most of those investigations were based on bulk composition of deposits which is not enough to understand the mechanisms involved in scavenging of metals from seawater (Lerche and Nozaki, 1998). Instead, separation of co-existing geochemical phases of ferromanganese oxides and determination of elemental composition of individual phases provides better information on the processes involved in their formation (Koschinsky and Halbach, 1995; Bau et al., 1996; Li, 1998; Koschinsky and Hein, 2003; Bau and Koschinsky, 2006; 2009). Selective chemical leaching techniques have been used to investigate solid-phase fractionation of different trace elements in ferromanganese oxides (Koschinsky and Halbach, 1995; Bau et al., 1996; Koschinsky and Hein, 2003; Takahashi et al., 2007; Bau and Koschinsky, 2009; Jiang et al., 2011). However, very few of the earlier investigations have focused on partitioning behavior of REEs (Bau et al., 1996; Bau and Koschinsky, 2009) and their mechanism of incorporation in solid oxides. Furthermore, no investigation on distribution of REEs among the solid phases of any hydrothermal Fe-Mn-oxide has been undertaken so far.

Here we present the results of REE composition in selectively leached fractions (viz., easily exchangeable phase, Mn-oxides, Fe-oxyhydroxides and residual phase) of both hydrothermal and hydrogenous ferromanganese oxides collected from Andaman Sea. This comparative study describes

how partitioning behavior of REEs differs among the common solid phases of two types of oxide. The oceanic processes and crystallographic effect of minerals responsible for different solid phase association of REEs and yttrium in these oxide samples has also been discussed.

2. Sampling locations and sample description

The Andaman basin is an active marginal back-arc basin in the northeastern Indian Ocean (Figure 1). Subduction of the Indian plate below the Southeast Asian plate led to the formation of this basin and the volcanic arc-trench system, marked by several geomorphological features such as an island arc, longitudinal faults, back-arc spreading centre and seamount complexes (Rudolfo, 1969; Kamesh Raju et. al., 2004; Kamesh Raju et. al., 2007). During a cruise (NIO-RVS-2) onboard *RV Sonne*, in November-December, 2007, multidisciplinary investigations including bathymetric survey, seafloor video imaging, and geological sampling were carried out in the Andaman volcanic-arc region. A submarine stratovolcano with well developed summit crater (the cratered seamount, CSM) was discovered in the Nicobar earthquake swarm area (Kattoju et al., 2008; Kamesh Raju et al., 2011) around 07°55'N and 94°03'E (Figure 1B). After bathymetric mapping and video observation, the rock samples were retrieved using TV-guided grab (TVG) and dredges (DR) from different parts of the volcanic seamount, CSM. Similar survey and seabed sampling were also carried out over another large seamount SM2 (the Southern seamount of Kamesh Raju et al., 2004) located around 10°N and 94°E, immediately south of the Andaman back-arc spreading center (ABSC) (Figure 1B).

All the rock samples from CSM and SM2 had thin (~2.0 mm) coating of ferromanganese oxides on their surfaces. Six ferromanganese oxide samples (three samples from each seamount) were selected for the present study. The details of sampling stations (Figures 1A, 1C and 1D) and physical nature of ferromanganese oxides are summarized in Table 1. The TVG-9G sample contains near spherical aggregates (average diameter 2.5 mm) of numerous sand-sized oxide globules embedded within the unconsolidated oxide layer on rocks of TVG-9. Biogenic remains (e.g. tests of foraminifera, radiolaria, broken shells of bivalves and gastropods) and pyroclastic particles were found within these globule aggregates, scanned under electron microscope (Kamesh Raju et al., 2011). To avoid contamination, the biological remains were separated from the aggregates under microscope. The ferromanganese encrustations from the summit (TVG-11) and flanks (TVG-12 and DR-06) of SM2 were hard, consolidated and thick (2.0 - 5.0 mm). All the ferromanganese oxide samples on the rock surface were

washed with Milli-Q® water and then scraped off carefully without cutting into the basal rock for onshore analysis.

In the present study, the results of the oxides from two seamounts of the Andaman Sea are compared with two well recognized deep-sea (water depth >5300 m) hydrogenous crusts (DR-12 and OG-116) from the Central Indian Ocean Basin (CIOB) (Figure 1A). These samples were obtained from the geological repository of the National Institute of Oceanography, Goa, India. The topmost layers (1.0 – 2.0 mm from surface), representing the recent part of the crust, were chosen for chemical analysis.

3. Analytical techniques

3.1. Mineralogical analysis

All the oxide and crust samples were powdered and analyzed for mineralogical composition using Rigaku X-ray diffractometer with Dmax-1c wide angle goniometer. Each sample was scanned thoroughly using Cu-K α radiation over 2θ ranging from 02° to 60°. Minerals were identified using MDI-JADE 5.0 search-match software.

3.2. Bulk geochemical analysis

For bulk chemical analysis, 50 mg of powdered samples were treated with 10 ml ultra-pure acid mixture ($HF:HNO_3:HClO_4$::7:3:1) in teflon beakers and then evaporated to dryness on a hot plate at 200°C. To this, 20 ml (1:1) diluted ultra-pure nitric acid was added and the final volume was adjusted to 250 ml with Milli-Q® water. Trace and rare earth element concentrations were measured with quadrupole ICP-MS (Perkin-Elmer SCIEX ELAN DRC-II) using ^{103}Rh solution (20 ng/ml) as internal standard (Balaram and Gnaneshwar Rao, 2003; Zahida et al., 2007). Concentrations of Fe and Mn in bulk samples were determined using Flame-AAS (Perkin-Elmer AAnalyst-200). An analytical accuracy of ~2.0% was routinely achieved against the marine reference standard material MAG-1 (Table 2 and 3) and precision was better than ±3.0%.

3.3. Iron isotope analysis

Fe isotope compositions of three representative samples, one from each seamount and one from CIOB, were measured with a Multi-Collector-ICP-MS (Nu plasma–HR from M/s. Nu Instruments, UK) at National Geophysical Research Institute, Hyderabad, India. Total Fe was separated from 50 mg of

digested samples using AG-MP1 anion-exchange resin and then eluted with 10 ml of 2.0(N) HCl and 0.001% H_2O_2 mixture. Iron recovery greater than 97% was achieved. The eluted fractions were evaporated and re-dissolved in 2.0% ultra-pure HNO_3. The isotopic analysis was carried out with Standard-Sample-Bracketing (SSB) mode (Albarede and Beard, 2004) using IRMM-014 as the standard reference material. Fe isotope results are reported in terms of relative isotopic ratios, $\delta^{56}Fe$ and $\delta^{57}Fe$, where $\delta^{x}Fe = [\{(^{x}Fe/^{54}Fe_{sample})/(^{x}Fe/^{54}Fe_{IRMM\text{-}014})\}\text{-}1]*10^{3}$, x = 56 or 57.

The standard deviation of replicate analyses lies within the limit of ±0.03‰ (1σ) for $\delta^{56}Fe$ and ±0.07‰ (1σ) for $\delta^{57}Fe$.

3.4. Sequential leaching and chemical analysis of leachates

Four major geochemical phases of all the oxide/crust samples were chemically separated following sequential leaching procedure (Koschinsky and Halbach, 1995; Koschinsky and Hein, 2003; Takahashi et al., 2007). In brief, 0.5 g of each powdered sample were thoroughly mixed with 15 ml of 1.0(M) acetic acid/Na-acetate buffer (pH = 5.0) solution and filtered through 0.45 µm Millipore® filter paper after shaking for five hours at room temperature. The filtrate (F-1) contains the loosely adsorbed elements which are easily exchangeable with seawater. The residues were further treated with 87.5 ml of 0.1(M) hydroxylamine hydrochloride solution (pH = 2.0) for 24 hours and then filtered to obtain fraction (F-2) associated with manganese oxides. The residues after filtration were stirred with 87.5 ml of 0.2(M) oxalic acid/ammonium oxalate buffer (pH = 3.5) solution for twelve hours and filtered to extract the third fraction (F-3) containing iron oxides and oxyhydroxides. The final fraction, which mostly contains the residual detrital phase (F-4) was completely digested with acid mixture ($HF:HNO_3:HClO_4$::7:3:1) at 200°C. All leaching experiments were carried out in a Class-1000 clean room at National Institute of Oceanography, Goa, India. Concentration of REEs and yttrium were measured in all four leachates of each sample with the same ICP-MS used for bulk analysis maintaining similar instrument operation and data acquisition parameters, mentioned by Zahida et al., (2007). The isobaric mass interferences of Ba-oxides during REE analysis (e.g., ^{136}BaO on ^{152}Sm and ^{137}BaO on ^{153}Eu) were corrected using metal oxide to metal ratio described by Lee et al. (2000). Recovery of elements (i.e., sum of REE-yttrium concentrations of four leachates divided by bulk concentrations) in leaching experiments was within the range of 86-114% (Appendix).

4. Results and discussion

4.1. Mineralogy, bulk geochemistry and growth rates of ferromanganese oxides: The genetic perspective.

The mineralogical analysis revealed that the ferromanganese oxides from CSM (TVG-9, TVG-9G and TVG-10) were more crystalline in nature and mostly dominated by 10Å manganate (Todorokite) with traces of other oxides like pyrolusite, birnessite and goethite (Table 1). Typical honeycomb-like surface feature (Figure 2) of todorokite was observed on TVG-9G globules under scanning electron microscope (Kamesh Raju et al., 2011). Several previous studies (Usui et al., 1986; Usui and Nishimura, 1992; Hodkinson et al., 1994; Buatier et al., 2004; Frank et al., 2006) had reported similar todorokite dominated Mn-oxide in low temperature hydrothermal deposits. On the contrary, oxides from SM2 (TVG-11, TVG-12 and DR-O6) showed the presence of poorly crystalline vernadite (δ-MnO_2) along with quartz. The mineralogical composition of the SM2 oxides resembled that of deep-sea crust samples (OG-116 and DR-12) from CIOB and other hydrogenous crusts from the Pacific (Hein et al., 1997) implying similarity in their genesis.

The bulk geochemistry of CSM oxides (TVG-9, TVG-9G and TVG-10) shows high concentration of Mn (24 - 35%), high Mn to Fe ratios (Mn/Fe = 4.0 -126) and low trace element (e.g. Cu, Co, Ni, Zr, Nb) content (Table 2). However, CSM oxides are rich in elements like Li and Mo (Table 2), which are soluble in hydrothermal fluid. This major and trace element composition of CSM oxides is very similar to that of low temperature (<100^{o}C) hydrothermal Fe-Mn-oxide deposits from the Kaikata Seamount (Usui and Nishimura, 1992), TAG vent field (Mills et al. 2001), Lesser Antilles volcanoes (Frank et al., 2006) and Lau basin (Paropkari et al., 2010). In contrast, SM2 oxides (TVG-11, TVG-12 and DR-O6) have low Mn content (7.5 – 13%), low Mn to Fe ratios (Mn/Fe = 0.4 - 0.7) but are relatively rich in trace elements (e.g. Co, Zr, Hf, Nb, Ta). Geochemical composition of SM2 oxides is comparable to that of CIOB crusts (Mn/Fe = 1.6 - 2.9, Table 2) and other hydrogenetic crusts (Banakar and Borole, 1991; Mills et al., 2001). Plots of geochemical data on the conventional ternary diagrams representing Fe-Mn-(Cu-Co-Ni)x10 and Fe-Mn-Cox100 systems (Figure 3) also show that CSM oxides are hydrothermal in nature while SM2 oxides are hydrogenous.

Trace element concentrations in ferromanganese oxides differ mainly due to the differences in their rate of precipitation and related scavenging processes (Kuhn et al., 2003). Thus concentration of a trace

element like cobalt in ferromanganese oxides is a useful marker for their growth rates (Halbach et al., 1983; Manheim, 1986; Manheim and Lane-Bostwick, 1988; Puteanus and Halbach, 1988). The growth rate of oxides having low cobalt concentration (Co < 8.0%) can be estimated following the empirical relation Growth rate $=6.8x10^{-1}/(Co^{n})^{1.67}$, where Co^{n} indicates cobalt concentration normalized to Fe and Mn contents (Manheim and Lane-Bostwick, 1988; Frank et al. 1999). Estimation of growth rates based on cobalt-chronology shows that CSM oxides precipitate at rates more than 1,400 mm/Myr (Table 2), which are similar to those of other well known hydrothermal deposits (e.g. Moore and Vogt, 1976; Ingram et al., 1990; Hodkinson et al., 1994; Fitzgerald and Gillis, 2006). Whereas, the growth of SM2 oxides (17 - 31.6 mm/Myr; Table 2) resembles those of typical hydrogenous crusts (average growth rate = 1.0 - 20 mm/Myr) reported by Segl et al. (1984), Puteanus and Halbach (1988), Ingram et al. (1990), Cowen et al. (1993).

The CSM oxide is rich in heavier Fe-isotopes (δ^{56}Fe = +0.21‰, δ^{57}Fe = +0.59‰; Kamesh Raju et al., 2011) relative to standard material, IRMM-014. Enrichment of heavy Fe-isotopes in CSM oxide can be explained by incomplete oxidation of $Fe(II)_{aqu}$ into $Fe(III)_{aqu}$ prior to hydrothermal oxide precipitation (Welch et al., 2003). During mixing with seawater lighter Fe-isotope rich $Fe(II)_{aqu}$ in hydrothermal fluid (Rouxel et al., 2003) is oxidized to heavier transient $Fe(III)_{aqu,}$ which in turn precipitates as solid Fe-oxyhydroxides. Experimental results on hydrothermal fluid showed ^{56}Fe-isotopic fractionation for [$Fe(III)_{aqu}$–$Fe(II)_{aqu}$] system at equilibrium is +3.44‰ (Severmann et al., 2004). Therefore, an isotopic fractionation of [Fe-oxyhydroxides–$Fe(III)_{aqu}$] less than that of [$Fe(III)_{aqu}$–$Fe(II)_{aqu}$], would generate heavier Fe-oxyhydroxides from lighter $Fe(II)_{aqu}$ solution. This is possible when fast precipitation of Fe-oxyhydroxides does not allow this process to attain equilibrium between the three Fe-species and makes all processes unidirectional and product oriented (Johnson and Beard, 2005). Nascent hydrothermal plume particulates from Rainbow field having unoxidised Fe(II) are characterized by heavier Fe-isotope composition (δ^{56}Fe = +0.15 to +1.2‰) relative to hydrothermal fluid (δ^{56}Fe = -0.23 ±0.09‰) (Severmann et al., 2004). Therefore enrichment of heavy Fe isotopes in the TVG-9G sample supports its extremely fast rate of precipitation as predicted by cobalt-chronology. In contrast, SM2 oxide is rich in lighter Fe-isotopes (δ^{56}Fe = -0.41‰, δ^{57}Fe = -0.72‰; Table 2). This isotopic composition is quite similar to that of CIOB crust (δ^{56}Fe = -0.53‰, δ^{57}Fe = -0.90‰; Table 2) and other deep-sea hydrogenous crusts (δ^{56}Fe = -0.8 to -0.0‰, Chu et al., 2006; δ^{57}Fe = -1.2 to -0.1‰; Levasseur et al., 2004). However, so far the reason for the lighter Fe-isotope composition of hydrogenous crust is not clear (Levasseur et al., 2004) but it is close to that in deep seawater (δ^{56}Fe = -0.14 to +0.32‰, Lacan et

al., 2008). This suggests that Fe-isotopes in hydrogenous ferromanganese-oxides directly reflect the Fe-isotopic composition of overlying seawater without much fractionation.

Thus, several strands of evidence including mineralogy, Mn/Fe ratio, growth rate, trace element and Fe-isotopic composition, confirm that the ferromanganese oxides collected from the CSM are low temperature hydrothermal type, while the SM2 oxides and CIOB crusts are purely hydrogenous.

4.2. Geochemistry of REEs and yttrium in ferromanganese oxides: Processes involved in hydrogenous and hydrothermal precipitation

4.2.1. Bulk REEs and yttrium composition

The hydrothermal (CSM) oxides have low REE-content (ΣREE <100 ppm) compared to hydrogenous SM2 oxides (ΣREE >1000 ppm) (Table 3). Enrichment of REEs in SM2 oxides (TVG-11, TVG-12 and DR-O6) matches well with those of CIOB crusts (DR-12, OG-116) and other hydrogenous crusts analyzed by Bau et al., (1996). Extremely slow growth rates allow hydrogenous oxides to scavenge REEs for longer times from seawater. Besides ΣREE, the Post-Archean Australian Shale (PAAS) normalized REE–yttrium patterns of the two types of oxide samples (Figure 4A) also differ in terms of Ce, Eu and Y-anomalies and light to heavy-REE fractionation (i.e., Nd_n/Yb_n). The CSM oxides are characterized by positive Eu (Eu/Eu* = 1.2 -1.9, Table 3), slightly negative Ce anomaly (Ce/Ce* < 1.0, Table 3) and relative enrichment of HREEs (Nd_n/Yb_n = 0.2 - 0.3, Table 3). This could be the result of oxidative precipitation of low temperature hydrothermal fluid. Similar observations on other hydrothermal oxides were reported by Hodkinson et al. (1994); Mills et al. (2001); Frank et al. (2006) and Paropkari et al. (2010). On the contrary, hydrogenous SM2 oxides and CIOB crusts exhibit significant positive Ce anomaly (Ce/Ce* > 1.0, Table 3) but negligible light to heavy-REE fractionation (Nd_n/Yb_n = 0.8 - 0.9, Table 3) and weak Eu-anomaly (Eu/Eu* = 0.92 - 1.2, Table 3). The positive Ce anomaly is due to the preferential removal of Ce(III) by settling particles (Kumar 1987).

The geochemical properties of yttrium are similar to those of heavy REEs and it is often referred to as pseudo-lanthanide. Like the REEs, the behavior of yttrium distinctly differs in the two types of oxides being investigated. Hydrogenous SM2 oxides have higher concentration of yttrium (61 – 132 ppm) than the hydrothermal CSM oxides (20 - 54 ppm) (Table 3). The SM2 oxides and CIOB crusts revealed negative Y-anomalies (Y_n/Ho_n = 0.6 – 0.7, Figure 4A) and have Y/Ho molar ratios between 30 and 40

(Table 3). Low particle reactivity and hence longer residence time of yttrium in seawater (compared to REEs, Zhang et al., 1994) are responsible for the negative Y-anomalies and low Y/Ho ratios in hydrogenous oxides, but positive Y-anomaly in seawater (Figure 4B). In striking contrast, the CSM oxides did not show any significant shale normalized Y-anomalies (Y_n/Ho_n = 0.9 -1.2). The high Y/Ho molar ratios (46 - 62, Table 3) are very similar to that in chondrite (Y/Ho ~52, Anders and Grevesse, 1989) and nascent particulates of hydrothermal plume (Y/Ho =42.5 - 61, Bau and Dulski, 1999 and references therein). This substantiates that the CSM oxides are purely hydrothermal and that they have received limited contribution from ambient seawater.

4.2.2. Relative abundance of REEs and yttrium in sequential leachates

The relative abundance (in percentage) of REEs and yttrium in four chemically separated leachates (e.g. exchangeable/loosely bound, Mn-oxide, Fe-oxyhydroxide and residual phases) of hydrothermal (CSM) and hydrogenous (SM2) oxides are shown in Figure 5A and 5B (Data in Appendix). For comparison, the results of simultaneously analyzed deep-sea hydrogenous crusts (DR-12 and OG-116) from CIOB are presented in Figure 5C (Data in Appendix). The sequential leaching experiment shows that REEs and yttrium in both hydrogenous and hydrothermal samples are mostly (~80% of total, Appendix) associated with two major oxide phases (F-2 and F-3) rather than exchangeable (F-1, <20% of total, Appendix) or residual (F-4, <10% of total, Appendix) phases. Low abundance of REEs in loosely bound phases of both types of oxide deposits suggests that these ferromanganese oxides deposited on seafloor, have little possibility to exchange REEs with ambient seawater. In hydrothermal CSM oxides, the Fe-oxyhydroxides act as principal host (~70% of total REE, Appendix) for most of the REEs (F-3, Figure 5A). Whereas, in hydrogenous SM2 oxides and CIOB crusts, rare earths are mostly associated with both easily reducible Mn-oxide and moderately reducible Fe-oxyhydroxide phases (F-2 and F-3, Figures 5B and 5C). The detrital materials which mostly represent the residual phase of both types of ferromanganese oxides contain extremely low REEs.

Thermodynamic calculations (Hass et al., 1995) as well as laboratory experiments (Lewis et al., 1998; Douville et al., 1999) show that dissolved REEs in geothermal fluid mostly occur as fluoride, chloride, sulfate complexes or free lanthanide ions, depending on availability of complex forming ions, temperature and pH of the parent fluid. It is interesting to note that although CSM oxides are rich in Mn, maximum REEs (except europium) and yttrium (~50 to 90% of total, Figure 5A, Appendix) are

associated with the amorphous Fe-oxyhydroxide phase. Such distribution of REEs and yttrium in hydrothermal oxides can be attributed to the preferential uptake of dissolved REE by Fe-oxyhydroxide particulates formed immediately after hydrothermal emission. German et al., (1990); Rudnicki and Elderfield (1992) and Glasby et al. (1997) described such effective REEs uptake mechanism by hydrothermal Fe-oxyhydroxide particulates in terms of co-precipitation during fluid-seawater mixing. In addition to co-precipitation, adsorption mediated by coulombic attraction also might play an important role in REE-partitioning among the geochemical phases of hydrothermal oxides. In an electrolyte medium, the pH_{zpc} (pH at zero point charge) of any solid adsorbent determines its surface charge density and thus adsorption efficiency for oppositely charged ions. Thus, amorphous Fe-oxyhydroxide (pH_{zpc} =8.5, Stumm and Morgan, 1981) forms in acidic hydrothermal fluid (pH < 7.0) would develop strong positive charge on its surface. A speciation calculation of REEs in low temperature (~25^{o}C) hydrothermal fluids from Endeavour field of the Juan de Fuca Ridge by Bao et al. (2008) shows that most (70 to 80% of total) of dissolved REEs and yttrium are present as sulfate, chloride and fluoride complexes, while the remaining 20 to 30% are free ions. In low temperature hydrothermal fluid, dissolved REE species would in all likelihood, exist as higher order neutral or negatively charged complexes, $Ln(SO_4)_2^-$, LnX_3^0 and LnX_4^-, (where X =Cl^- or F^-) and may be expected to be strongly adsorbed on to Fe-oxyhydroxide phase. Thus, both co-precipitation and coulombic attraction mediated surface adsorption make F-3, the Fe-oxyhydroxide phase of CSM oxides, the primary host for REEs leaving other phases (i.e, F-1, F-2 and F-4) as poor adsorbents.

Compared to TVG-9 and TVG-9G oxides from the CSM flank (ΣREE = 45 - 65 ppm, Fe <1.0%), sample TVG-10 collected from inside the crater is relatively enriched in Fe (6.1%) and REEs (ΣREE = 91 ppm). This result clearly indicates that due to the non-conservative nature of Fe and REEs in hydrothermal fluid, the dissolved REEs were co-precipitated rapidly along with Fe-oxyhydroxides inside the crater. Low REE and Fe concentrations in TVG-9 and TVG-9G oxides on the flank suggest that hydrothermal precipitation decreases away from the source as the fluid is diluted through mixing with ambient seawater. However, high ΣREE/Fe ratios (~5.0 - $23.2x10^{-3}$, Table-3) with decreased Fe concentration of TVG-9 and TVG9G samples compared to TVG-10 (ΣREE/Fe ~$1.4x10^{-3}$, Table-3) indicate that even though the rate of co-precipitation drops, hydrothermal particulates continue to adsorb dissolved REEs from seawater as they are dispersed from the source. Similar behavior of suspended particles was reported in TAG (German et al., 1990; 1991; Rudnicki and Elderfield, 1993) and EPR (Sherrell et al., 1999) hydrothermal plumes.

In hydrogenous ferromanganese oxides incorporation of REEs from seawater occurs mainly through scavenging processes following complex mechanisms including electrostatic attraction and chemical interaction as described by Koeppenkastrop and De Carlo (1992). These hydrogenous ferromanganese oxides are mainly composed of poorly crystalline vernadite in association with Fe-oxyhydroxide and traces of detrital materials. In seawater dissolved REEs are mostly present as mono-carbonate, $Ln(CO_3)^+$ or di-carbonate, $Ln(CO_3)_2^-$ species (Byrne and Kim, 1990; Byrne and Sholkovitz, 1996). At seawater pH (~ 7.9) the colloidal Mn-oxide phase (pH_{zpc} = 2.0 - 2.8; Stumm and Morgan, 1981) of hydrogenous crust would develop strong negative surface potential and preferentially attract positively charged mono-carbonate complexes of lanthanides, $Ln(CO_3)^+$. Relatively less abundant free lanthanide ions $Ln^{3+}_{(aqu)}$ or other minor complexes like $LnSO_4^+$, $LnOH^{+2}$, $LnCl^{+2}$ in seawater are also likely to be adsorbed onto Mn-oxide phases. Theoretical studies and laboratory experiments also revealed Mn-oxide as the best adsorbent of REEs from seawater or similar electrolyte medium (Ohta and Kawabe, 2000a). The amorphous Fe-oxyhydroxides (pH_{zpc} = 8.5), which might develop slightly positive surface charge in seawater (pH ~ 7.9), would adsorb negatively charged species, mostly $Ln(CO_3)_2^-$. Thus a major fraction of REEs in hydrogenous crust is distributed in both Fe and Mn-oxide phases.

The Mn-oxide phase of hydrogenous oxides has more LREEs than HREEs and there is an overall decreasing trend in abundance from La to Lu (F-2 in Figures 5B and 5C) unlike the Fe-oxyhydroxide phase which shows an opposite trend (F-3 in Figures 5B and 5C). Our observation agrees well with experimental results obtained by Ohta and Kawabe, (2001). Such affinities for particular solid phases can be explained in terms of relative abundance of carbonate complexes of REEs in seawater. Byrne (2002) explained the relative abundances of carbonate species of REEs in seawater in terms of their carbonate complexation equilibrium and pH of seawater. According to his study, REE-carbonate complexes with higher equilibrium constants are more stable and abundant in seawater. In slightly alkaline pH of seawater, the stability constants and estimated abundance of negatively charged di-carbonates, $Ln(CO_3)_2^-$ gradually increases with increasing atomic number of the lanthanides (Ohta and Kawabe, 2000). This is apparently the cause for progressive enrichment of lanthanides from La to Lu in hydrogenous Fe-oxyhydroxide (F-3) phase and a gradual drop in their concentrations in the Mn-oxide (F-2) phase. The plots of relative stability of di-carbonate complexes over mono-carbonates in seawater, (i.e, $\log(\beta^0_2/\beta^0_1)$, Ohta and Kawabe, 2000) show a negative relationship (r = -0.92) (Figure 6A) with the

abundance of REEs in the Mn-oxide phase but a positive relationship (r=+0.86) (Figure 6B) with REEs adsorbed in Fe-oxyhydroxide. Furthermore, the abundances of REEs in both oxide phases display a sigmoidal pattern which can be subdivided into four contiguous curved sections (Figures 6A and 6B). The four sections of these curves provide compelling evidence for the change in stability of REE-complexes due to the tetrad effect representing quarter, half, three-quarter and completely filled 4f orbitals of elements over the lanthanide series. Ohta and Kawabe (2000) also emphasized that the tetrad effect is associated with REE-carbonate complexation constants and corresponding distribution coefficients between ferromanganese-oxide and seawater. The good correlations between the relative stability of carbonate-species of rare earths and their abundances in two oxide phases suggest that REE-speciation in seawater is the prime controlling factor for solid phase distribution of REEs in hydrogenous crust. Our present observation is in agreement with the results presented by Varentsov et al. (1991) for Krylov seamount crust.

Besides REE-speciation in seawater, the mineralogy of oxide deposits may also have a role in partitioning of REEs among the geochemical phases of ferromanganese oxides (Bau and Koschinsky, 2009). Particularly, the large differences between REE abundances in F-2 phase of hydrogenous and hydrothermal oxides could be due to their different Mn-oxide mineral composition. Vernadite (δ-MnO_2), the main Mn-oxide mineral in hydrogenous Fe-Mn-oxide has a layered structure composed of MnO_6 octahedra (Post, 1999). It has been proposed that the space between randomly stacked layers of vernadite accommodates various heavy metal cations which also compensate the negative surface charge of these layers (Manceau et al., 2002; Peacock and Sherman, 2007; Sherman and Peacock, 2010). A similar crystallographic effect might facilitate sorption of REEs (particularly cationic LREE-species) on hydrogenous Mn-oxides. Triclinic birnessite (β-MnO_2) of hydrothermal oxide also has a layered structure of octahedral MnO_6 yet, unlike vernadite, it does not possess any inter-layer vacant site to hold any cations except manganese ions (Peacock and Sherman, 2007). Other hydrothermal manganese minerals, todorokite and pyrolusite, contain small chains or tunnels of edge-sharing MnO_6 octahedra which hardly accommodate any chemical species (Post, 1999). Thus crystal structures of birnessite, pyrolusite and todorokite are another considerable factor favoring low ΣREE of hydrothermal oxides.

4.2.3. Shale normalized REE-yttrium-patterns of sequential leachates

The PAAS normalized REE-yttrium patterns of four chemically separated leachates of hydrothermal and hydrogenous oxides are shown in Figure 7. Hydrogenous oxides of SM2 and deep-sea crusts from CIOB have identical REE-patterns in all four leaches. This indicates that hydrogenous oxides have similar exchange equilibria for REE between seawater and solid phases, irrespective of sample locations and depth regimes. However, the REE-patterns of Mn-oxide, the F-2 phase of hydrogenous SM2 and CIOB samples drastically differ from those of hydrothermal CSM oxides and on the log scale these patterns are separated by an order of magnitude or more (Figure 7B). This difference in REE association with Mn-oxide phases of two types of oxides apparently reflects the difference in ΣREE of bulk samples as discussed earlier. Besides ΣREE, other characteristic features in bulk REE-patterns of the two types of ferromanganese oxides (e.g. Eu, Ce, Y-anomalies and heavy to light REE fractionation) are found to be associated with one or two particular phases of these oxides. The REE-patterns of loosely bound, F-1 (Figure 7A) and residual, F-4 (Figure 7D) phases of both types of oxides are quite similar.

A positive Eu-anomaly appears mainly in Mn-oxide, (F-2) of hydrothermal oxides (Figure 7B). In hydrothermal fluid, unlike other lanthanides, dissolved europium is mostly present as free Eu^{+2} ions (Haas et al., 1995). Of course, the Eu-anomalies in REE-patterns of TVG-9G and TVG-10 samples are not very clear but considering the reliability of low REE concentration data, we can ascertain that positively charged Eu^{+2} ions would be adsorbed onto negatively charged Mn-oxides. This electrostatic attraction possibly causes considerable enrichment of Eu (>30% of total, Figure 5A) and positive Eu-anomalies (Eu/Eu* = 2.5 - 6.5, Appendix) in the Mn-oxide phase of hydrothermal CSM samples. The residual phase (Figure 7D) of all the samples revealed flat REE-patterns with minor positive Eu-anomalies (Eu/Eu* = 1.2 - 3.8, Appendix) irrespective of sample type. Both the hydrogenous and hydrothermal ferromanganese oxides are known to contain traces of detrital refractory minerals such as quartz and feldspar (Koschinsky and Hein, 2003) which normally represent their residual (F-4) phase. Feldspars are known to form more stable complexes with Eu^{+2} rather than trivalent lanthanides (MÖller and Muecke, 1984) and are responsible for positive Eu anomalies in the residual phase.

Acetate buffer soluble loosely bound-REE fractions (F-1) in both types of oxides have pronounced negative Ce-anomalies (Ce/Ce* = 0.01- 0.29, Appendix) (Figure 7A). For hydrogenous crusts, these results are contrast with corresponding bulk REE-patterns (Figure 4A) which have positive Ce

anomalies. In hydrogenous crusts Ce is mostly present as Ce(IV)-oxide which would hardly dissolve in weak acetate buffer but needs strong reducing agents (e.g. hydroxylamine hydrochloride or ammonium oxalate) to convert into soluble Ce(III). This can explain the observed negative Ce-anomaly in the loosely bound phase and positive Ce-anomalies in both Mn-oxide (Ce/Ce* = 1.7 - 3.2, Appendix) (Figure 7B) and Fe-oxyhydroxide phases (Ce/Ce* = 1.9 – 8.3, Appendix) (Figure 7C). The positive Ce-anomalies in Mn-oxide and Fe-oxyhydroxide phases suggest that oxidation of dissolved Ce(III), followed by adsorption of Ce(IV) has taken place on both the metal-oxides. Furthermore, the quite comparable size of these Ce-anomalies indicates both the oxides play equally important roles in Ce-oxidation in seawater. This observation does not agree with the earlier studies which showed that the positive Ce anomaly is due to oxidative scavenging of Ce by Mn-oxide (e.g. Kumar 1987; Elderfield 1988; Moffet 1990; DeCarlo and McMurtry 1992) but not by the Fe-oxyhydroxide. Nevertheless, the experimental results (Ohta and Kawabe, 2001) and estimated oxide phases-seawater partition co-efficients for REEs (Bau and Koschinsky, 2009) revealed that both Mn-oxide and Fe-oxyhydoxide phases may possess positive Ce-anomalies. The oxide minerals of hydrothermal deposits did not show any particular trends in Ce-anomalies, when the data are normalized to shale. Slightly negative or lack of any Ce-anomalies in two oxide phases of CSM samples might be due to the slow rate of oxidative sorption of Ce(III) on fast growing Fe-Mn-oxide particulates in reduced hydrothermal end member fluid.

Negative Y-anomalies in shale normalized patterns of the bulk samples of hydrogenous oxides (Figure 4A) have appeared in the Fe-oxyhydroxide (F-3) phase (Figure 7C). Although trivalent yttrium has a similar size the HREEs its speciation in seawater is different from that of the HREEs. In seawater (pH = 7.9) carbonate complexes of HREEs are dominated by di-carbonate species $Ln(CO_3)_2^-$ while yttrium occurs as more positively charged monocarbonate (YCO_3^+) (Byrne, 2002 Bau and Koschinsky 2009). Therefore, compared to yttrium, HREEs are scavenged more on positively charged Fe-oxyhydroxide surfaces, resulting in negative Y- anomalies (Y_n/Ho_n =0.4-0.7, Appendix) in F-3 fraction of hydrogenous oxides. Broadly there is no major Y-anomaly (Y_n/Ho_n = 0.8 - 1.5, Appendix) (except F-2 phase of TVG-9G) in four phases of CSM samples (Figure 7). This suggests that yttrium and HREEs behave similarly during hydrothermal precipitation and these elements have identical speciation in hydrothermal fluid. Bau and Dulski (1999) also mentioned that speciation of yttrium and REEs in hydrothermal fluid are dominated by halide complexes and free ions.

The shale normalized REE-patterns of four phases of hydrogenous oxides (Figure 7) do not show any fractionation between light and heavy REEs, but the Fe-oxyhydroxide phase of hydrothermal oxides is relatively rich in HREEs (Nd_n/Yb_n =0.25-0.29, Appendix) (Figure 7C). Abundant neutral or negatively charged fluoride or chloride complexes of rare earths in hydrothermal fluid would adsorb on positively charged surfaces of Fe-oxyhydroxide colloids. At low temperature, the stability of such halides (particularly fluoride complexes) increases with increasing atomic number (Haas et al., 1995). Thus more stable halides of HREEs in hydrothermal fluid would preferentially adsorb on Fe-oxyhydroxide. This is perhaps responsible for light to heavy REE-fractionation in F-3 fraction of CSM oxides (Figure 7C).

5. Conclusion

Based on our present investigations on partitioning of REEs and yttrium among the co-existing solid phases of hydrothermal and hydrogenous oxides it can be concluded that:

(1) The ferromanganese oxides of hydrothermal and hydrogenous origin have unique and distinctly different distributions of REEs and yttrium in their geochemical phases. The great majority of total REEs and yttrium of these ferromanganese oxides is mainly associated with Mn-oxide and Fe-oxyhydroxide phases rather than with easily exchangeable and residual phases. In hydrothermal oxides, REEs and yttrium are mostly associated with Fe-oxyhydroxide but in hydrogenous oxides, both Mn-oxide and Fe-oxyhydroxide phases are important hosts for the REEs, with the LREE and HREE preferentially adsorbed onto Mn-oxide and Fe-oxyhydroxide, respectively.

(2) A major fraction of total REEs and yttrium in hydrothermal oxides co-precipitates along with Fe-oxyhydroxide particulates immediately after hydrothermal emission. With time co-precipitation of REE reduces as fluid gets diluted with seawater while adsorption of REE on hydrothermal particulates increases away from the source. The hydrogenous oxides have identical solid phase distribution of REEs and yttrium irrespective of location, water depth, tectonic setting and physical nature of the samples. Therefore it can be suggested that adsorption of REE-carbonate species from seawater is the predominant mechanism for REE-partitioning in hydrogenous oxides.

(3) The layered structure of vernadite in hydrogenous oxides can accommodate REE species whereas todorokite, birnessite and pyrolusite in hydrothermal oxides allow hardly any REE-species within their

crystal structure. Thus crystallography of Mn-oxides also effectively contributes to controlling total REE content and their partitioning behavior in two types of ferromanganese oxide.

(4) Distribution of yttrium markedly differs from that of REEs in phases of hydrogenous oxides but not in hydrothermal oxides. Mono-carbonate dominated yttrium speciation in seawater makes its partitioning behavior different from that of di-carbonate dominated HREEs in hydrogenous oxides. In contrast, identical speciation of yttrium and REEs in hydrothermal fluid maintains analogous partitioning behavior for the different geochemical phases of hydrothermal oxide.

Acknowledgement

The authors are thankful to the Directors of the National Institute of Oceanography, Goa and National Geophysical Research Institute, Hyderabad, for their support and encouragement. We thank the Head, Department of Earth Sciences, IITB, for supporting this work. We are grateful to Dr. M. Dileep Kumar for his valuable comments to improve the manuscript, Ms. Kiranmai Samudrala for preparing bathymetric maps and Mr. V. D. Khedekar for SEM-EDS analysis. Authors are also thankful to Dr. Y. J. Bhaskar Rao and Mr. B. Vijaya Gopal, NGRI for providing MC-ICPMS facility. The crew members onboard *R/V Sonne* are thanked for their assistance during the cruise. Mr. Surya Prakash thanks CSIR, India for Senior Research Fellowship. We thank Dr. Rachel A. Mills and anonymous reviewers for their constructive comments. This is NIO contribution XXXX.

References

Albarede, F., Beard, B.L., 2004. Analytical methods for nontransitional isotopes. In: Johnson, C.M., Beard, B.,L. and Albarede, F. (Eds.), Geochemistry of Non-transitional Stable Isotopes. Reviews in Mineralogy and Geochemistry, vol. 55, pp. 113-152.

Aplin A.C., Cronan D.S., 1985. Ferromanganese oxide deposits from the Central Pacific Ocean, I. Encrustations from the Line Island Archepelago. Geochim. Cosmochim. Acta. 49, 427-436.

Anders, E., Grevesse, N., 1989. Abundances of the elements: Meteoritic and solar. Geochim. Cosmochim. Acta 53, 197-214.

Balaram, V., Gnaneshwar Rao, T., 2003. Rapid determination of REEs and other trace elements in geological samples by microwave acid digestion and ICP-MS. Atomic Spectro. 24, 206-212.

Banakar, V.K., Borole, D.V., 1991. Depth profiles of ^{230}Th excess, transition metals and mineralogy of ferromanganese crusts of the Central Indian basin and implications for paleo-oceanographic influence on crust genesis. Chem. Geol. 94, 33-44.

Bao, S., Zhou, H., Peng, X., Ji., F., Yao, H., 2008. Geochemistry of REE and yttrium in hydrothermal fluids from the Endeavour segment, Juan de Fuca Ridge. Geochem. J. 42, 359-370.

Bau, M., Koschinsky, A., Dulski, P., Heinz, J.R., 1996. Comparison of the partitioning behaviors of yttrium, rare earth elements, and titanium between hydrogenetic marine ferromanganese crusts and seawater. Geochim. Cosmochim. Acta 60, 1709- 1725.

Bau, M., Dulski, P., 1999. Comparing yttrium and rare earths in hydrothermal fluids from the Mid-Atlantic Ridge: implications for Y and REE behavior during near-vent mixing and for the Y/Ho ratio of Protrusion seawater. Chem. Geol. 155, 77-90.

Bau, M., Koschinsky, A., 2006. Hafnium and neodymium isotopes in seawater and in ferromanganese crusts: The "element perspective". Earth Planet. Sci. Lett. 241, 952-961.

Bau, M., Koschinsky, A., 2009. Oxidative scavenging of cerium on hydrous Fe oxide: Evidence from the distribution of rare earth elements and yttrium between Fe oxides and Mn oxides in hydrogenetic ferromanganese crusts. Geochem. J. 43, 37-47.

Buatier, M.D., Guillaume, D., Wheat, C.G., Herve, L., Adatte, T., 2004. Mineralogical characterization and genesis of hydrothermal Mn oxides from the flank of the Juan the Fuca Ridge. American Mineral. 89, 1807-1815.

Byrne, R.H., Kim, K.H., 1990. Rare earth element scavenging in seawater. Geochim. Cosmochim. Acta 54, 2645–2656.

Byrne, R.H., Sholkovitz 1996. Marine chemistry and geo-chemistry of the lanthanides. In: Gschneider, K.A., and Eyring, L. (Eds.), Handbook of physics and chemistry of Rare Earths. Elsevier, vol. 23, pp. 497-592.

Byrne, R.H., 2002. Inorganic speciation of dissolved elements in seawater: the influence of pH on concentration ratios. Geochem. Trans. 3, 11-16.

Calvert, S.E., Cronan D.S., 1978. Geochemistry of oceanic ferromanganese deposits [and discussion]. Phil. Trans. Roy. Soc. London. A290, 43-73.

Chu, N.C., Johnson, C.M., Beard, B.L., German, C.R., Nesbitt, R.W., Frank, M., Bohn, M., Kubik, P.W., Usui, A., Graham, I., 2006. Evidence of hydrothermal venting in Fe-isotope compositions of the deep Pacific Ocean through time. Earth Planet. Sci. Lett. 245, 202-217.

Cowen, J.P., de Carlo, E.H., McGee, D.L., 1993. Calcareous nannofossil biostratigraphic dating of ferromanganese crust from Schumann seamount. Mar. Geol. 115, 289-306.

DeCarlo, E.H., McMurtry, G.M., 1992. Rare-earth geochemistry of ferromanganese crusts from the Hawaiian Archipelago, central Pacific. Chem. Geol. 95, 235-250.

Douville, E., Bienvenu, P., Charlou, J.L., Donval, J.P., Fouquet, Y., Appriou, P., Gamo, T., 1999. Yttrium and rare earth elements in fluids from various deep-sea hydrothermal systems. Geochim. Cosmochim. Acta 63, 627–643.

Elderfield, H., Hawkesworth, C. J., Greaves, M. J., Calvert, S. E., 1981. Rare earth element geochemistry of oceanic ferromanganese nodules and associated sediment. Geochim. Cosmochim. Acta 45, 513 - 528.

Elderfield, H., 1988. The oceanic chemistry of the rare earth elements. Phil. Trans. Roy. Soc. London A325, 105 -126.

Fitzgerald, C.E., Gillis, K.M., 2006. Hydrothermal manganese oxide deposits from Baby Bare seamount in the Northeast Pacific Ocean. Mar. Geol. 225, 145 – 156.

Frank, M., O'Nions, R.K., Hein, J.R., Banakar, V.K., 1999. 60 Myr records of major elements and Pb–Nd isotopes from hydrogenous ferromanganese crusts: Reconstruction of seawater paleochemistry. Geochim. Cosmochim. Acta 63, 1689-1708.

Frank, M., Marbler, H., Koschinsky, A., Flierdt, T. van de, Klemm, V., Gutjahr, M., Halliday, A.N., Kubik, P.W., Halbach, P., 2006. Submarine hydrothermal venting related to volcanism in the Lesser Antilles: Evidence from ferromanganese precipitates. Geochem. Geophys. Geosystems 7, 1-24. doi:10.1029/2005GC001140.

Friedrich, G., Schmitz-wiechowski, A., 1980. Mineralogy and chemistry of a ferromanganese crust from a deep-sea hill, Central Pacific, "Valdivia" cruise VA13/2. Mar. Geol. 37, 71-90.

German, C.R., Klinkhammer, G.P., Edmond, J.M., Mitra, A., Elderfield, H., 1990. Hydrothermal scavenging of rare-earth elements in the ocean. Nature 345, 516-518.

German, C.R., Campbell, A.C., Edmond, J.M., 1991. Hydrothermal scavenging at the Mid-Atlantic Ridge: Modification of trace element dissolved fluxes. Earth Planet. Sci. Lett. 107, 101-114.

Glasby, G.P., 1973. Mechanisms of enrichment of the rarer elements in marine manganese nodules. Mar. Chem. 1, 105-125.

Glasby, G.P., Stuben, D., Jeschke, G., Stoffers, P., Garbe-Sch~Nberg, C.D., 1997. A model for the formation of hydrothermal manganese crusts from the Pitcairn Island hotspot. Geochim. Cosmochim. Acta 61, 4583-4597.

Glasby, G.P., 2000. Manganese: predominent role of nodules and crusts. In: Schulz, H.D. and Zabe, M. (Eds.), Marine Geochemistry. Springer, Berlin, pp. 335-372.

Haas, J.R., Shock, E.L., Sassani, D.C., 1995. Rare earth elements in hydrothermal systems: estimates of standard partial molal thermodynamic properties of aqueous complexes of the rare earth elements at high pressures and temperatures, Geochim. Cosmochim. Acta 59, 4329–4350.

Halbach, P., Segl, M., Puteanus, D., Mangini, A., 1983. Co-fluxes and growth rates in ferromanganese deposits from central Pacific seamount areas. Nature 304, 716– 719.

Hein, J.R., Koschinsky, A., Halbach, P., Manheim, F.T., Bau, M., Kang, J.K., Lubick, N., 1997. Iron and manganese oxide mineralisation in the Pacific. In: Nicholson, K., Hein, J.R., Buhn, Ž.B.,

Dasgupta, S. (Eds), Manganese Mineralisation: Geochemistry and Mineralogy of Terrestrial and Marine Deposits. Geol. Soc. Spec. Publ., vol. 119, pp. 123 –138.

Hodkinson, R.A., Stoffers, P., Scholten, J., Cronan, D.S., Jeschke, G., Rogers, T.D.S., 1994. Geochemistry of hydrothermal manganese deposits from the Pitcairn Island hotspot, southeastern Pacific. Geochim. Cosmochim. Acta 58, 5011 – 5029.

Ingram, B.L., Hein, J.R., Farmer, G.L., 1990. Age determinations and growth rates of Pacific ferromanganese deposits using strontium isotopes. Geochim. Cosmochim. Acta 54, 1709-1721.

Jiang, X.J., Lin, X.H., Yao, D., Guo, W.D., 2011. Enrichment mechanisms of rare earth elements in marine hydrogenic ferromanganese crusts. Sci. China Earth Sci. 54, 197-203.

Johnson, C.M., Beard, B.L., 2005. Biogeochemical cycling of iron isotopes. Science 309, 1025-1027.

Kamesh Raju, K.A., Ramprasad, T., Rao, P.S., Ramalingeswara, Rao B., Varghese, J., 2004. New insights into the tectonic evolution of the Andaman basin, northeast Indian Ocean. Earth Planet. Sci. Lett. 221, 145-162.

Kamesh Raju, K.A., Murty, G.P.S., Amarnath, D., Mohan Kumar, M. L., 2007. The west Andaman fault and its influence on the aftershock pattern of the recent megathrust earthquakes in the Andaman-Sumatra region. Geophys. Res. Lett. 34, L03305, doi: 10.1029/2006GL028730.

Kattoju, K.R., Ray, D., Mudholkar, A., Gollu, M.P., Mathew, R., Paropkari, A.L., Kalathil B., Ramachandran R., 2008. Tectonic and magmatic implications of the off-Nicobar earthquake swarm, Andaman Sea. *Eos Trans.* AGU, 89(53), AGU Fall Meet. Suppl, (Abstract T51B-1890).

Kamesh Raju, K.A., Ray, D., Mudholkar, A.V., Murty, G.P.S., Gahalaut, V.K., Kiranmai Samudrala, Paropkari, A.L., Ramachandran R., Surya Prakash L., 2011. Tectonic and volcanic implications of a cratered seamount off Nicobar Island, Andaman Sea. (Communicated).

Koeppenkastrop, D., DeCarlo, E.H., 1992. Sorption of REEs from seawater onto synthetic mineral particles: An experimental approach. Chem. Geol. 95, 251-263.

Koschinsky, A., Halbach, P., 1995. Sequential leaching of marine ferromanganese precipitates: Genetic implications. Geochim. Cosmochim. Acta 59, 5113-5132.

Koschinsky, A., Hein, J.R., 2003. Uptake of elements from seawater by ferromanganese crusts: solid-phase associations and seawater speciation. Mar. Geol. 198, 331-351.

Kuhn,T., Bostick, B.C., Koschinsky, A., Halbach, P., Fendorf, S., 2003. Enrichment of Mo in hydrothermal Mn precipitates: possible Mo sources, formation process and phase associations. Chem. Geol. 199, 29-43.

Kumar M. D., 1987. Cation hydrolysis and the regulation of trace metal composition in seawater. Geochim. Cosmochim. Acta 51, 2137-2145.

Lacan, F., Radic, A., Jeandel, C., Poitrasson, F., Sarthou, G., Pradoux, C., Freydier, R., 2008. Measurement of isotopic composition of dissolved iron in the open ocean. Geophys. Res. Lett. 35, doi: 10.1029/2008GL035841.

Lee, K., Shishido, S., Kusachi, I., Motomizu ,S., 2000. Determination of lathanoids and yttrium in JGb2 and JR3 by inductively coupled plasma-mass spectrometry after cation-exchange pretreatment. Geochem. J. 34, 383-393.

Lerche, D., Nozaki, Y., 1998. Rare earth elements of sinking particulate matter in the Japan Trance. Earth Planet. Sci. Lett. 159, 71-86.

Levasseur, S., Frank, M., Hein, J.R., Halliday, A.N., 2004. The global variation in the iron isotope composition of marine hydrogenetic ferromanganese deposits: implications for seawater chemistry? Earth Planet. Sci. Lett. 224, 91-105.

Lewis, A.J., Komninou, A., Yardley, B.W.D., Palmer, M.R., 1998, Rare earth elements speciation in geothermal fluids from Yellowstone National Park, Wyoming, USA. Geochim. Cosmochim. Acta 62, 657-663.

Li, Y.H., 1998. Distribution patterns of the elements in the ocean: A synthesis. Geochim. Cosmochim. Acta 55, 3223-3240.

Manceau, A., Lanson, B., Drits, V.A., 2002. Structure of heavy metal sorbed birnessite: Part III. Results from powder and polarized extended X-ray absorption fine structure spectroscopy. Geochim. Cosmochim. Acta 66, 2639-2663.

Manheim, F.T., 1986. Marine cobalt recourses. Science 232, 600-608.

Manheim, F.T., Lane-Bostwick, C.M., 1988. Cobalt in ferromanganese crusts as a monitor of hydrothermal discharge on the Pacific sea floor. Nature 335, 59–62.

Mills, R.A., Wells, D.M., Roberts, S., 2001. Genesis of ferromanganese crusts from the TAG hydrothermal field. Chem. Geol. 176, 283-293.

MÖller, P., Muecke, G.K., 1984. Significance of Europium anomalies in silicate melt and crystal-melt equilibria : a re-evaluation. Contrib. Mineral. Petrol. 87, 242-250.

Moffett J.W., 1990. Microbially mediated Ce-oxidation in seawater. Nature 345, 421-423.

Moorby, S.A., Cronan, D.S., 1981. The distribution of elements between co-existing phases in some marine ferromanganese-oxide deposits. Geochim. Cosmochim. Acta 45, 1855-1877.

Moore, W.S., Vogt, P.R., 1976. Hydrothermal manganese crusts from two sites near the Galapagos spreading axis. Earth Planet. Sci. Lett. 29, 349-356.

Nath, B.N., Balaram, V., Shudhakar, M., Plüger W.L., 1992. Rare earth element geochemistry of ferromanganese deposits from the Indian Ocean. Mar. Chem. 38, 185-208.

Nath, B.N., Pluger, W.L., Roelandts, I., 1997. Geochemical constraints on the hydrothermal origin of ferromanganese encrustations from the Rodriguez Triple Junction, Indian Ocean. In Manganese mineralization: Geochemistry and mineralogy of terrestrial and marine deposits. eds. by: Nicholson, K.; Hein, J.R.; Buhn, B.; Dasgupta, S.(Geol. Soc. Spec. Publ.; 119). Geological Society; London; UK; 1997; 199-211.

Ohta, A., Kawabe, I., 2000. Rare earth element partitioning between Fe oxyhydroxide precipitates and aqueous NaCl solutions doped with $NaHCO_3$: Determinations of rare earth element complexation constants with carbonate ions. Geochem. J. 34, 439-454.

Ohta, A., Kawabe, I., 2000a. Theoretical study of tetrad effects observed in REE distribution coefficients between marine Fe-Mn deposit and deep seawater, and in REE (III)-carbonate complexation constants. Geochem. J. 34, 455-473.

Ohta, A., Kawabe, I., 2001. REE(III) adsorption onto Mn dioxide (δ-MnO_2) and Fe oxyhydroxide: Ce(III) by δ-MnO_2. Geochim. Cosmochim. Acta 65, 695–670.

Paropkari, A.L., Ray, D., Balaram, V., Surya Prakash, L., Mirza, I.H., Satyanarayana, M., Rao, T.G., Kaisary, S., 2010. Formation of hydrothermal deposits at Kings Triple Junction, northern Lau back-arc basin, SW Pacific: The geochemical perspectives. J. Asian Earth Sci. 38, 121-130.

Peacock, C.L., Sherman, D.M., 2007. Sorption of Ni by birnessite: Equilibrium controls on Ni in seawater. Chem. Geol. 238, 94-106.

Post, J.E., 1999. Manganese oxide minerals: Crystal structures and economic and environmental significance. Proc. Natl. Acad. Sci. 96, 3447-3454.

Puteanus, D., Halbach, P., 1988. Correlation of Co concentration and growth rate – A method for age determination of ferromanganese crusts. Chem. Geol. 69, 73-85.

Rajani, R.P., Banakar, V.K., Parthiban, G., Mudholkar, A.V., Chodankar, A.R., 2005. Compositional variation and genesis of ferromanganese crusts of the Afanasiy-Nikitin Seamount, Equatorial Indian Ocean. J. Earth Syst. Sci. 114, 51-61.

Rouxel, O., Dobbek, N., Ludden, J., Fouquet, Y., 2003. Iron isotope fractionation during oceanic crust alteration. Chem. Geol. 202, 155-182.

Rudnicki, M.D., Elderfield, H., 1993. A chemical model of the buoyant and neutrally buoyant plume over the TAG vent field, 26 degrees N, Mid-Atlantic Ridge. Geochim. Cosmochim. Acta 57, 2939-2957.

Rudolfo, K.S., 1969. Bathymetry and marine geology of the Andaman basin and tectonic implications for SE Asia. Geol. Soc. Am. Bull. 80, 1203-1230.

Segl, M., Mangini, A., Bonani, G., Hofmann, H.J., Nessi, M., Suter, M., Wolfli, W., Friedrich, G., Pluger, W.L., Wiechowski, A., Beer, J., 1984. ^{10}Be dating of a manganese crust from Central North Pacific and implications for ocean paleocirculation. Nature 309, 540–543.

Shermann, D.M., Peacock, C.L., 2010. Surface complexation of Cu on birnessite (δ-MnO_2): Controls on Cu in the deep ocean. Geochim. Cosmochim. Acta 74, 6721-6730.

Sherrell, R.M., Field, M.P., Ravizza, G., 1999. Uptake and fractionation of rare earth elements on hydrothermal plume particles at 9°45'N, East Pacific Rise. Geochim. Cosmochim. Acta 63, 1709-1722.

Severmann, S., Johnson, C.M., Beard, B.L., German, C.R., Edmonds, H.N., Chiba, H., Green, D.R.H., 2004. The effect of plume processes on the Fe isotope composition of hydrothermally derived Fe in the deep ocean as inferred from the Rainbow vent site, Mid-Atlantic Ridge, 36°14'. Earth Planet. Sci. Lett. 225, 63-76.

Stumm, W., Morgan, J.J., 1981. An introduction emphasizing chemical equilibria in natural waters. In: Aquatic Chemistry (2nd edit.), John Wiley and Sons, New York.

Takahashi, Y., Manceau, A., Geoffroy, N., Marcus, M.A., Usui, A., 2007. Chemical and structural control of the partitioning of Co, Ce and Pb in marine ferromanganese oxides. Geochim. Cosmochim. Acta 71, 984–1008.

Toth, J.R., 1980. Deposition of submarine crusts rich in manganese and iron. Bull. Geol. Soc. Am. 91, 44 -54.

Usui, A., Yuasa, M., Yokota, S., Nohara, M., Nishimura, A., Murakami, F., 1986. Submarine hydrothermal manganese deposits from the Ogasawara (Bonin) Arc, off the Japan Islands. Mar. Geol. 73, 311-322.

Usui, A., Nishimura, A., 1992. Hydrothermal manganese deposits from the Izu- Ogasawara (Bonin) - Mariana Arc and adjacent areas. Bull. Geol. Survey Jap. 43, 257-284.

Varentsov, I.M., Drits, V.A., Gorshkov, A.I., 1991. Rare earth element indicators of Mn-Fe oxyhydroxide crust formation on Krylov Seamount, Eastern Atlantic. Mar. Chem. 96, 71-84.

Welch, S.A., Beard, B.L., Johnson, C.M., Braterman, P.S., 2003. Kinetic and equilibrium Fe isotope fractionation between aqueous Fe(II) and Fe(III) Geochim. Cosmochim. Acta 67, 4231-4250.

Zahida, B., Balaram, V., Ahmad, S.M., Satyanarayanan, M., Gnaneshwar Rao, T., 2007. Determination of Trace and Rare Earth Elements in Marine Sediment Reference Materials by ICP-MS: Comparison of Open and Closed Acid Digestion Methods. Atomic Spectro. 28, 41-50.

Zhang, J., Amakawa, H., Nozaki, Y., 1994. The comparative behaviors of yttrium and lanthanides in the seawater of the north Pacific. Geophys. Res. Lett. 21, 2677–2680.

Figure captions:

Figure 1: (A) Sampling locations (⊕) of ferromanganese crusts from Central Indian Ocean Basin (CIOB). The inset shows the locations of two seamounts (★) in the Andaman Sea. (B) The enlarged version of inset as in A showing detailed bathymetry and locations of seamounts ( ) in the Andaman Sea (C) Bathymetric map of Southern seamount, SM2, south of Andaman Back-arc Spreading Centre, ABSC, showing the locations of ferromanganese oxides TVG-11, TVG-12 and DR-06 (D) Bathymetry of the Cratered seamount, CSM in earthquake swarm area off Nicobar Island with sampling locations of ferromanganese oxides TVG-9 and TVG-10.

Figure 2: Scanning Electron Microscope image and Energy dispersive spectrum of globular Manganese-oxide (TVG-9G) collected from the flank of the Cratered seamount (CSM) in Nicobar earthquake swarm area (from Kamesh Raju et al., 2011).

Figure 3: Ternary diagrams of Fe-Mn-(Cu+Ni+Co)x10 and Fe-Mn-Cox100 (e.g., Toth, 1980; Usui and Nashimura, 1992; Nath et al., 1997; Frank et al., 2006) systems to classify the genetic origin of ferromanganese oxides. Both the plots are indicating dominant hydrothermal source for CSM ferromanganese oxides (TVG-9, TVG-9G and TVG-10) and hydrogenous source for SM2 ferromanganese oxides (TVG-11, TVG-12 and DR-06) and CIOB crusts (DR-12 and OG-116).

Figure 4: Shale (PAAS) normalized bulk REE - yttrium patterns of (A) ferromanganese oxides from the CSM (TVG-9, TVG-9G and TVG-10) (data from Kamesh Raju et al. 2011), SM2 (TVG-11, TVG-12 and DR-06), CIOB crusts (DR-12 and OG-116) and (B) typical deep seawater (data from Bao et al., 2008) for comparison.

Figure 5: Comparative REE - yttrium abundances in four leachates (Easily exchangeable, Mn-oxide, Fe-oxyhydroxide and Residual) of ferromanganese oxides from the (A) CSM (TVG-9, TVG-9G and TVG-10), (B) SM2 (TVG-11, TVG-12 and DR-06) and (C) CIOB crusts (DR-12 and OG-116).

Figure 6: Correlation between stability constants of REE - carbonate complexes with the fraction of total REEs associated with (A) Mn-oxide and (B) Fe-oxyhydroxide phase. The stability constant data for REE - carbonates were taken from Ohta and Kawabe (2000). The trends of REE abundance in both the phases have sigmoidal appearance with distinct tetrad effect (dashed lines) across the lanthanide series.

Figure 7: Shale (PAAS) normalized REE - yttrium patterns of four sequential leachates, (A) Easily exchangeable/loosely adsorbed, (B) Mn-oxide, (C) Fe-oxyhydroxide and (D) Residual phases, of ferromanganese oxides from CSM (TVG-9, TVG-9G and TVG-10), SM2 (TVG-11, TVG-12 and DR-06) and CIOB crusts (DR-12 and OG-116).

Figure 1

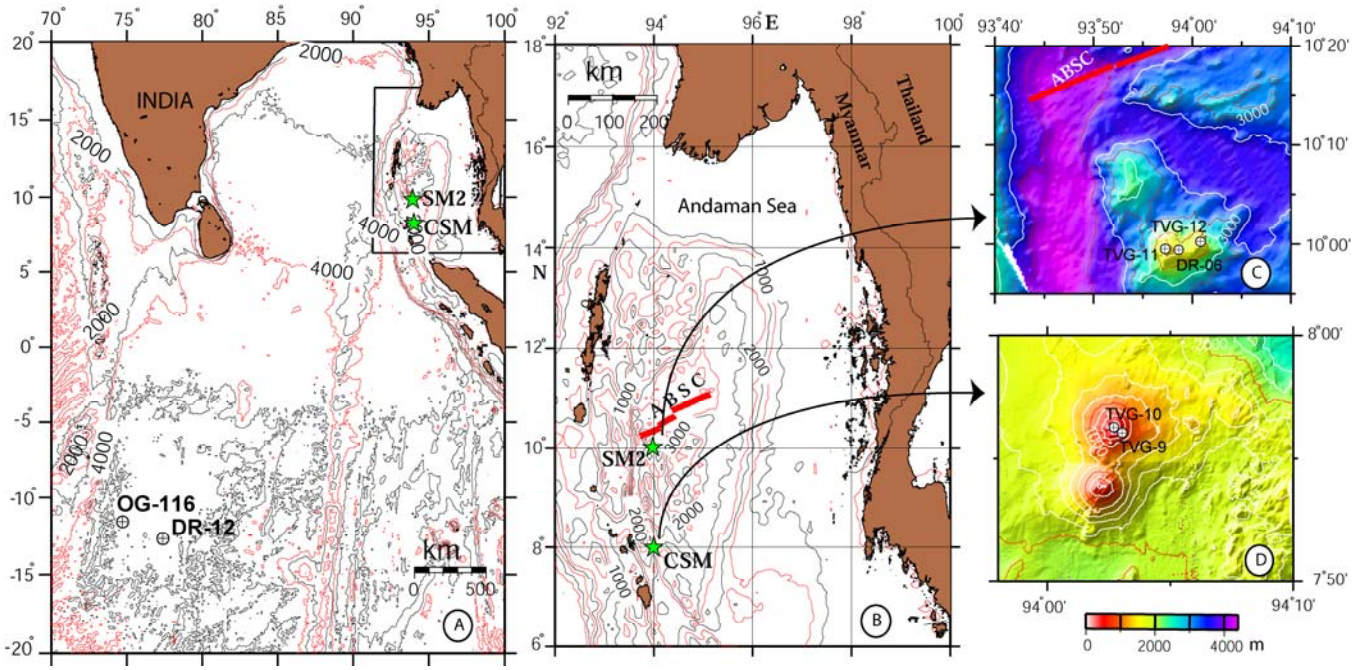

Figure 2

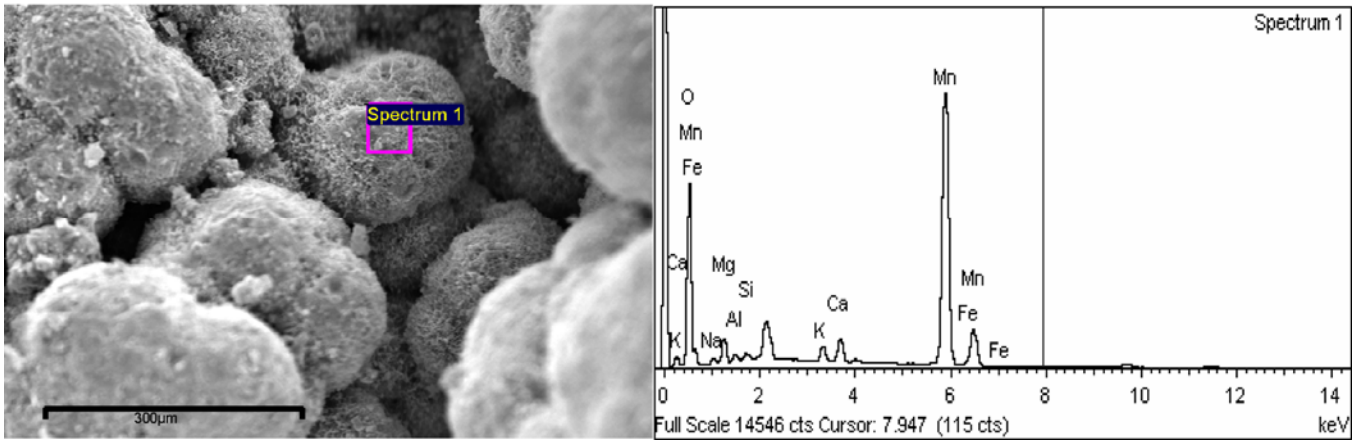

Figure 3

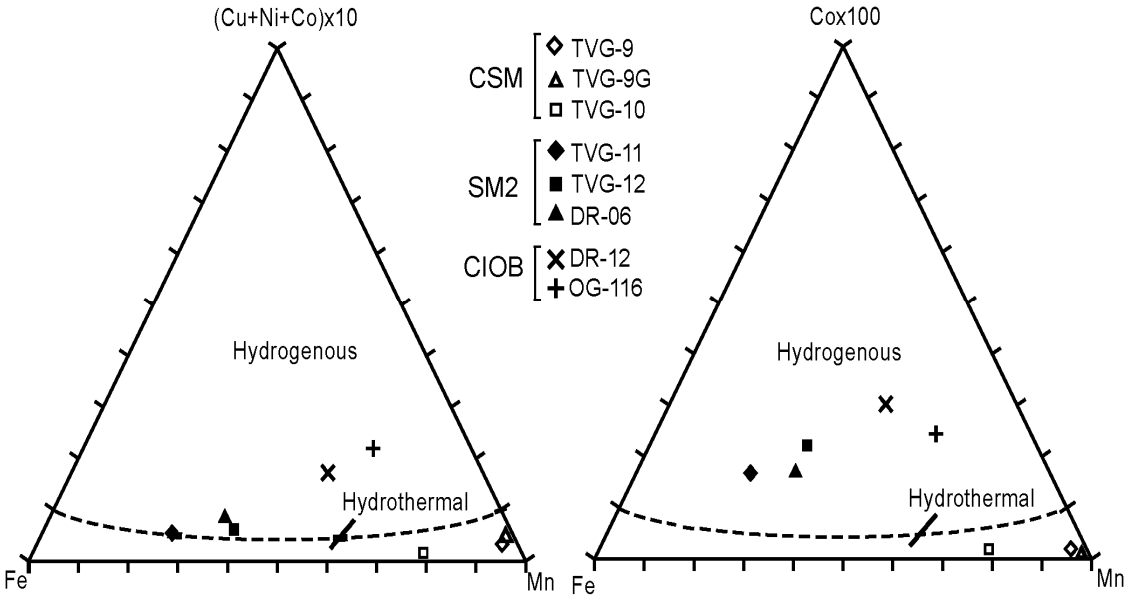

Figure 4

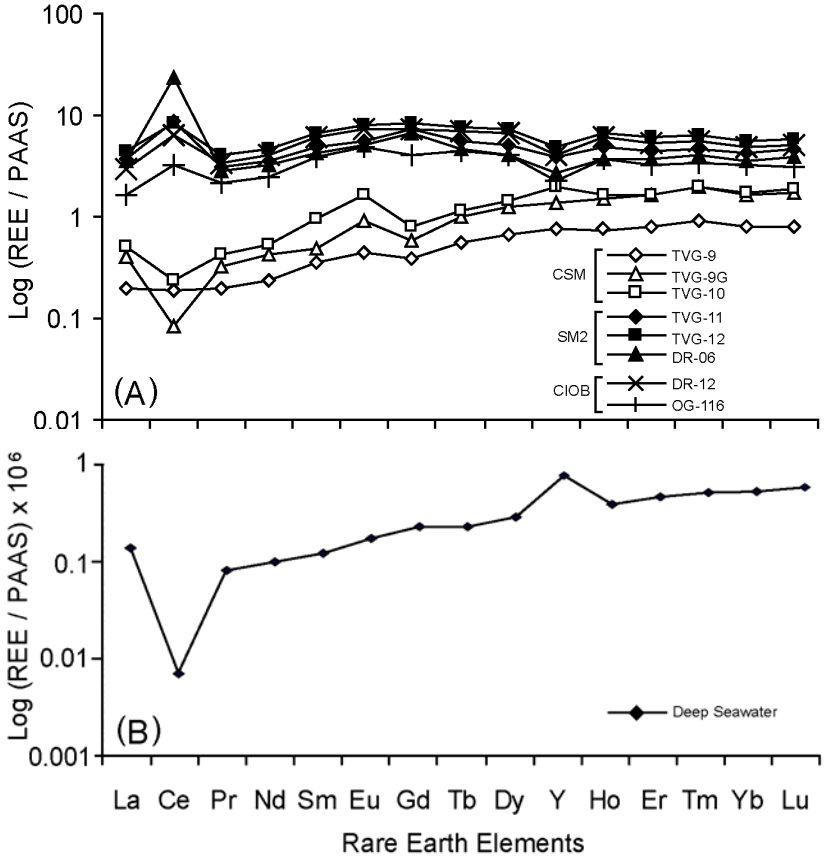

Figure 5

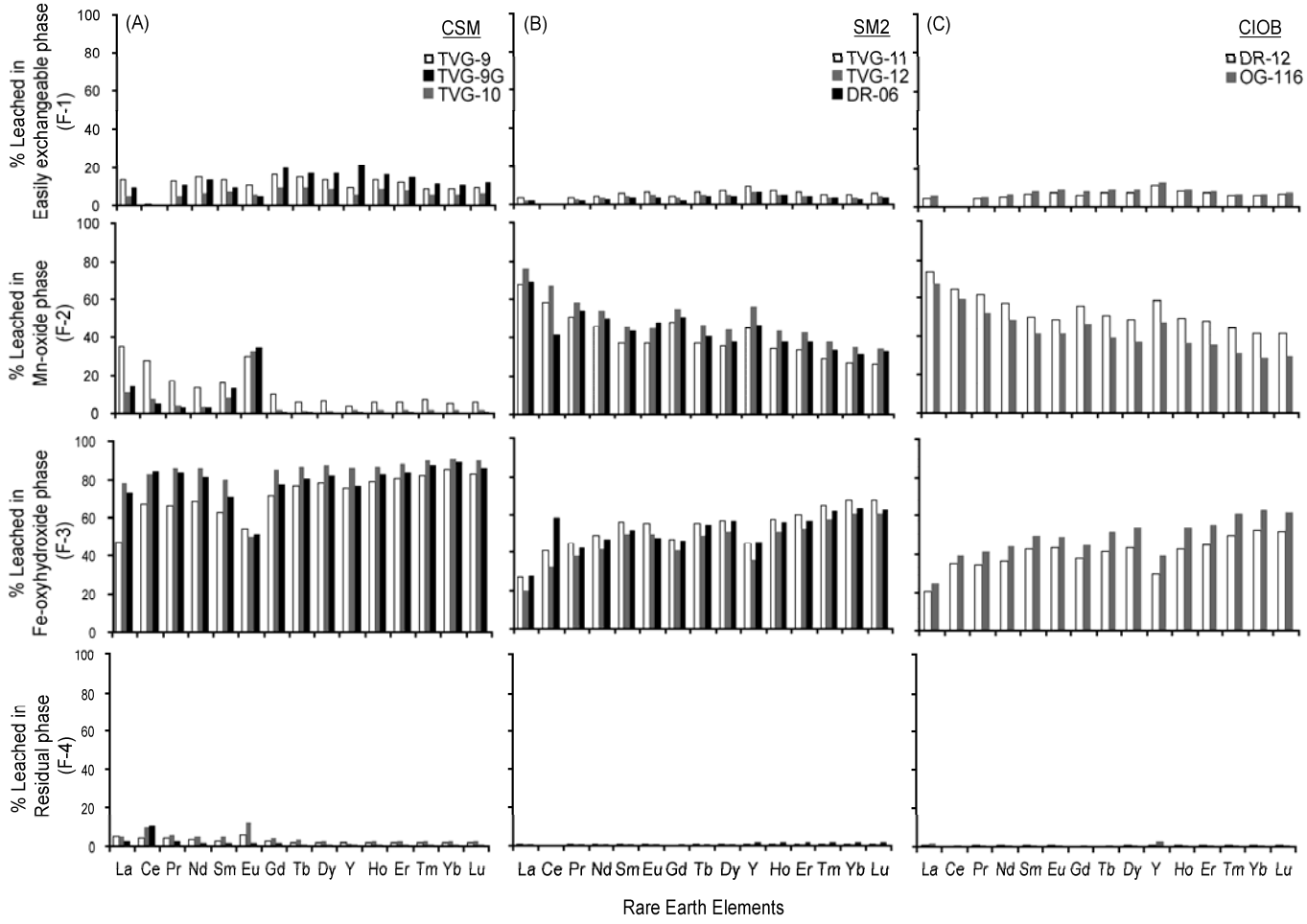
(A)
CSM
TVG-9
TVG-9G
TVG-10
(B)
SM2
TVG-11
TVG-12
DR-06
(C)
CIOB
DR-12
OG-116
% Leached in Easily exchangeable phase (F-1)
% Leached in Mn-oxide phase (F-2)
% Leached in Fe-oxyhydroxide phase (F-3)
% Leached in Residual phase (F-4)
0
20
40
60
80
100
La Ce Pr Nd Sm Eu Gd Tb Dy Y Ho Er Tm Yb Lu
Rare Earth Elements

Figure 6

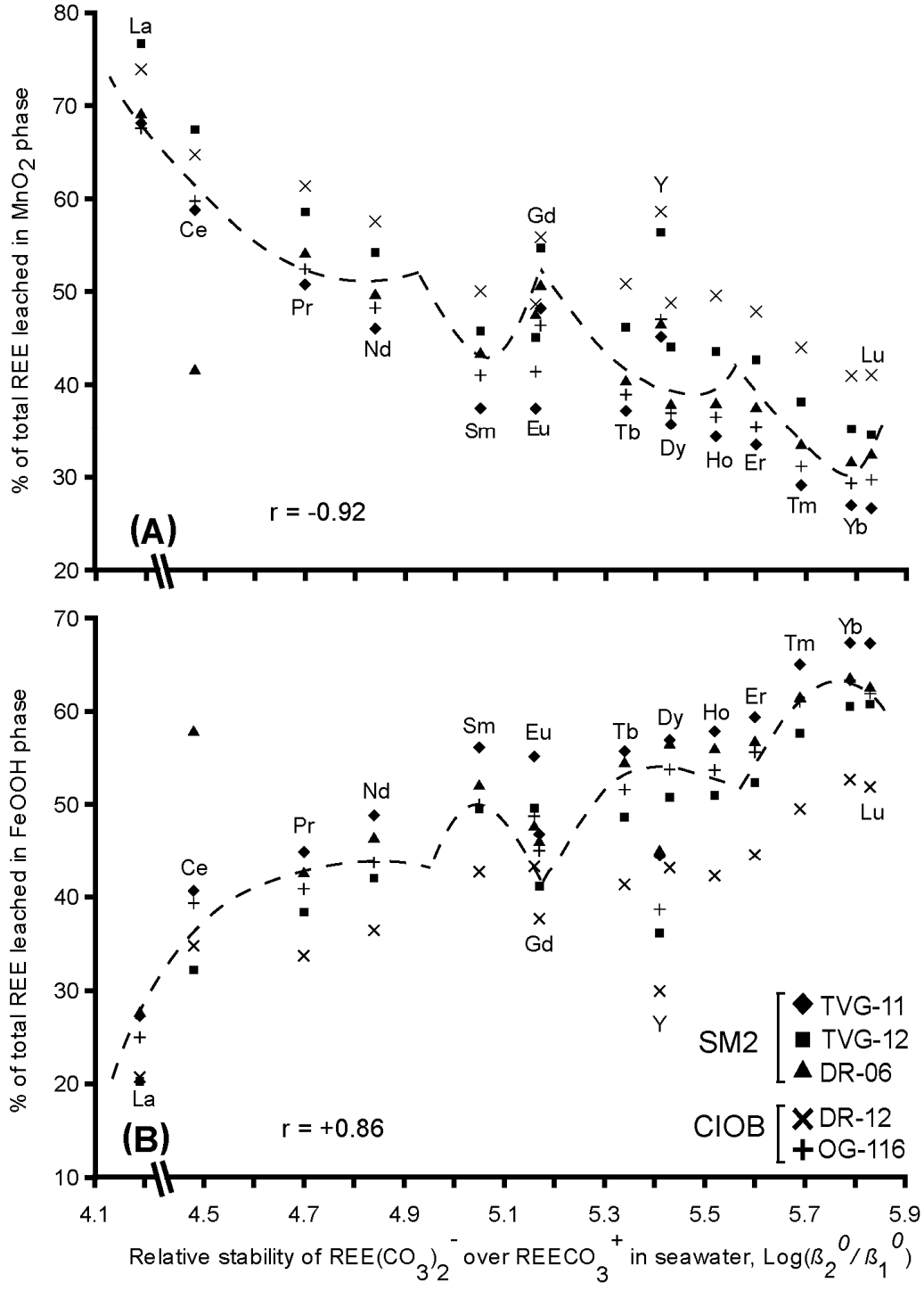
% of total REE leached in MnO2 phase
% of total REE leached in FeOOH phase
(A)
(B)
r = -0.92
r = +0.86
La
Ce
Pr
Nd
Sm
Eu
Gd
Tb
Dy
Y
Ho
Er
Tm
Yb
Lu
SM2
TVG-11
TVG-12
DR-06
CIOB
DR-12
OG-116
Relative stability of REE(CO3)2- over REECO3+ in seawater, Log(ß2 0/ß1 0)

Figure 7

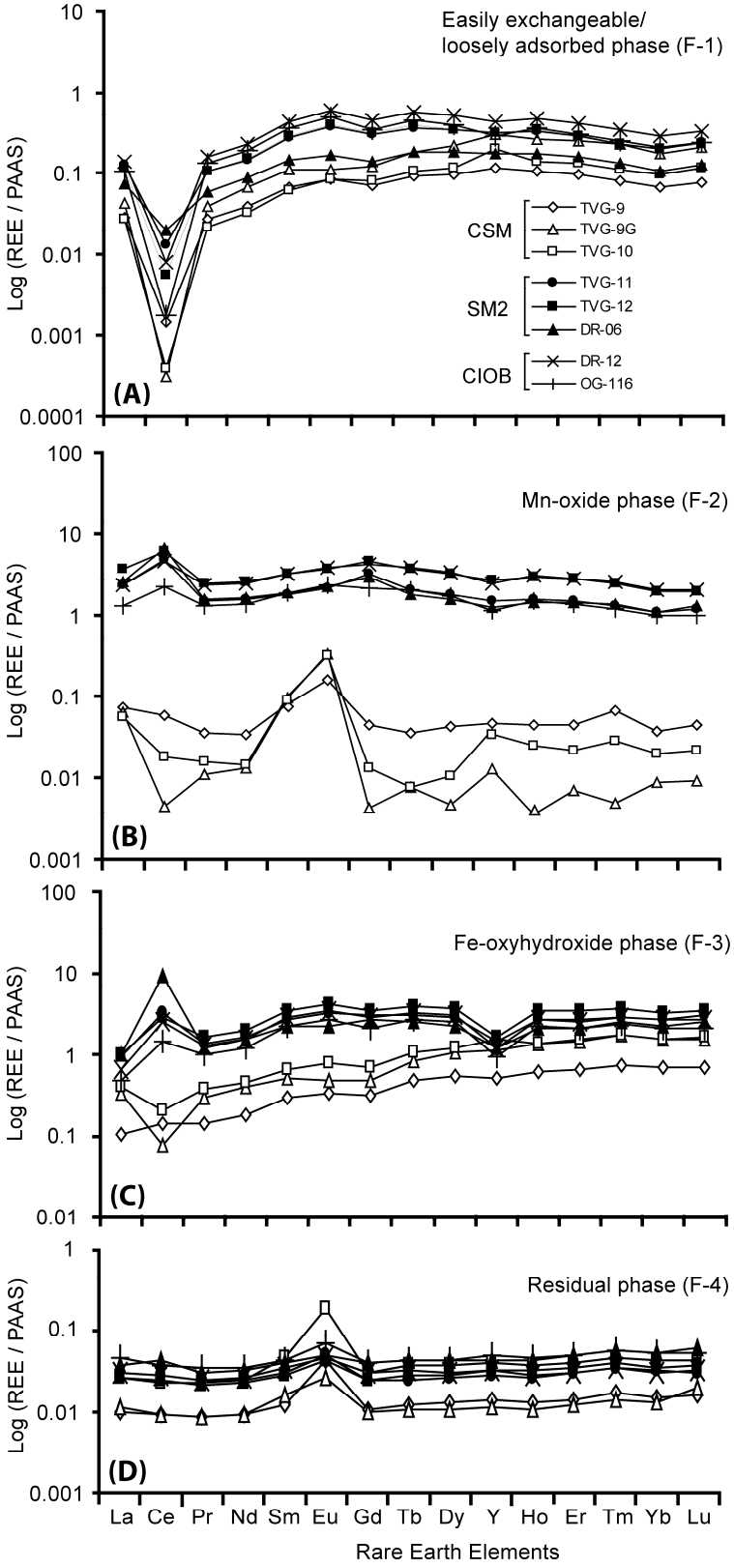
Easily exchangeable/
loosely adsorbed phase (F-1)
CSM
TVG-9
TVG-9G
TVG-10
SM2
TVG-11
TVG-12
DR-06
CIOB
DR-12
OG-116
(A)
Mn-oxide phase (F-2)
(B)
Fe-oxyhydroxide phase (F-3)
(C)
Residual phase (F-4)
(D)
Log (REE / PAAS)
La Ce Pr Nd Sm Eu Gd Tb Dy Y Ho Er Tm Yb Lu
Rare Earth Elements

Table 1. : Sample descriptions and mineralogy of ferromanganese oxides.

Cruise No. and Sample ID	Sampling Location (Lat., Long.)	Water depth (m)	Sample description	Mineralogy
Cratered seamount (CSM)				
NIO-RVS-II TVG-9	07°55.924'N 94°03.139'E	511	Unconsolidated dusty Fe-Mn-oxide coating on rocky substratum from the slope of submarine volcano in Nicobar swarm area.	10Å manganate (todorokite) and birnessite with traces of quartz, pyrolusite, and calcite.
NIO-RVS-II TVG-9G	07°55.924'N 94°03.139'E	511	Fragile hemispheroidal sand size globules found to be associated with ferromanganese coatings of TVG-9. SEM images revealed the presence of biogenic remains (e.g. tests of foraminifera, radiolarian, broken shells of bivalves and gastropods) within the globule aggregates.	10Å manganate and birnessite.
NIO-RVS-II TVG-10	07°56.33'N 94°02.638'E	398	Unconsolidated thin Fe-Mn-oxide coating on pebbles collected from the crater floor of same underwater volcano.	10Å manganate and birnessite with goethite and pyrolusite
Southern seamount (SM2)				
NIO-RVS-II TVG-11-3b	09°59.5'N 93°57.137'E	1299	Ferromanganese encrustations on rocks recovered from the summit of southern seamount (SM2) near the back-arc spreading ridge system in Andaman basin.	Quartz dominates over Vernadite (δMnO_2).
NIO-RVS-II TVG-12-1a	10°00.243'N 94°00.784'E	1455	About 4.0-5.0mm thick Fe-Mn oxide coatings cemented on rocks from the smaller peak of same seamount in further north.	Vernadite and Quartz
AAS-11 DR-06	09°59.45'N 93°58.97'E	1640	Hard ferromanganese oxide encrustations on rock samples recovered from the deeper flank area within the two peaks of the same seamount.	Vernadite and Quartz
Central Indian Ocean Basin (CIOB)				
AAS-26 DR-12	12°32.484'S 75°40.902'E	5375	Surface layer of deep sea crust from Central Indian Ocean basin.	Vernadite and Quartz
ABP-002 OG-116	11°48.744'S 75°45.001'E	5310	Surface layer of deep sea crust from Central Indian Ocean basin.	Quartz and Vernadite

10Å manganate: $(Na, Ca, K)_2 (Mn^{4+}, Mn^{3+})_6O_{12}.H_2O$, Pyrolusite: β-MnO_2,
Birnessite: $(Na.Ca)_{0.5} (Mn^{4+}, Mn^{3+})_2O_4.1.5H_2O$, Goethite: α-FeO(OH), Quartz: SiO_2.

Table 2.: Bulk geochemical compositions and relative growth rates of ferromanganese oxides from the Andaman Sea and deep-sea crusts from the Central Indian Ocean Basin (CIOB). Data for CSM is from Kamesh Raju et al. (2011). The growth rate based on 'cobalt chronology' were estimated following the empirical relation [Growth rate = $6.8x10^{-1}/ (Co^{n})^{1.67}$] where Co^{n} indicates cobalt concentration normalized to Fe and Mn contents (e.g, Manheim and Lane-Bostwick, 1988).

Elements	Cratered seamount (CSM)			Southern seamount (SM2)			Central Indian Ocean Basin (CIOB)		USGS Reference standard MAG-1	
(ppm)	TVG-9	TVG-9G	TVG-10	TVG-11	TVG-12	DR-06	DR-12	OG-116	Certified values	Mean of 05 analyses
Li	198.4	474.3	62.8	21.3	25.6	NA	41.9	71.8	79	80.04
Sc	3.31	4.05	4.64	14.1	11.9	14	10.9	7.36	17.2	17.16
V	227.9	180.1	242.3	444.8	476.6	424.1	358.4	294.9	140	139.6
Cr	9.14	15.3	13.5	23.6	14.4	38.2	7.23	9.01	97	97.09
Co	57.5	19.8	59.5	538.3	765.3	669.8	1089	746	20	20.45
Ni	843.1	1232	398.2	685.2	941.7	2207	3110	3956	53	53.08
Cu	57.1	151.1	12.5	30.4	65.5	157.8	1037	1797	30	31.02
Zn	311.9	545.7	123.9	167	223.1	384.1	289.2	396.8	130	129.5
Rb	3.34	6.47	4.54	8.2	6.78	11.3	8.35	9.79	149	148.5
Sr	303.7	517.8	467.3	648.2	802.3	610.8	468.7	347.6	146	144.0
Cs	0.075	0.29	0.13	0.402	0.44	0.826	0.31	0.391	8.6	8.59
Mo	80.9	414.7	145.1	46.5	89.5	166.9	104.3	120.4	1.6	1.59
Zr	27.1	34.6	45	398.4	368.3	470.1	468.9	294.7	126	124.3
Nb	1.25	0.706	0.994	27.7	22.9	47	20.7	10.7	12	11.83
Hf	0.67	0.47	0.669	9.58	7.53	14.6	9.65	5.35	3.7	3.66
Ta	0.002	0.057	0.033	0.479	0.399	0.262	0.441	0.234	1.1	1.12

Pb	19.3	24.3	55.1	627.9	619	ND	280.3	165.9	24	24.39
Th	0.849	0.806	0.911	59	55.7	106	45.4	25.4	11.9	11.8
U	2.14	3.34	3.19	4.09	5.33	5.42	3.04	2.06	2.7	2.72
Mn (%)	27.2	35.4	24.2	7.4	11	12.7	15.7	17.3	0.076	0.076
Fe (%)	0.91	0.28	6.1	19.4	16	20.3	9.5	5.86	4.58	4.61
Mn/Fe	29.9	126.4	3.97	0.38	0.68	0.62	1.65	2.95	-	-
Co/Zn	0.18	0.03	0.48	3.22	3.43	1.74	3.76	1.88	-	-
Th/U	0.39	0.24	0.28	14.4	10.4	19.5	14.9	12.3	-	-
δ^{56}Fe (‰) ± 1σ	NA	0.21± 0.031	NA	NA	-0.412± 0.022	NA	NA	-0.531± 0.022	-	-
δ^{57}Fe (‰) ± 1σ	NA	0.599± 0.063	NA	NA	-0.720± 0.037	NA	NA	-0.904± 0.053	-	-
Growth rate (mm/Myr)	1432	12657	1534	31.6	17.7	31	8.78	14.35	-	-

NA = Not Analyzed, ND = Not Detected

Table 3. : Bulk REE- yttrium concentrations and systematics of ferromanganese oxides from the Andaman Sea and deep-sea crusts from the Central Indian Ocean Basin (CIOB). Data for CSM is from Kamesh Raju et al. (2011).

Elements	Cratered seamount (CSM)			Southern seamount (SM2)			Central Indian Ocean Basin (CIOB)		USGS Reference standard MAG-1	
(ppm)	TVG-9	TVG-9G	TVG-10	TVG-11	TVG-12	DR-06	DR-12	OG-116	Certified values	Mean of 05 analyses
La	7.35	15.81	19.55	138.6	166.9	137.4	110.8	62.85	43	41.87
Ce	15.06	6.57	19.01	680.7	654.6	1930	514.7	255.7	88	87.35
Pr	1.7	2.86	3.76	27.2	35.11	25.31	30.37	19.01	9.3	9.257
Nd	8.11	14.64	17.73	119.3	157.2	109.1	135.2	84.1	38	37.20
Sm	1.955	2.635	5.4	26.42	36.19	24.01	33.52	21.36	7.5	7.55
Eu	0.483	0.966	1.78	6.11	8.49	5.48	7.75	5.28	1.55	1.531
Gd	1.8	2.68	3.65	34.21	39.61	30.99	33.35	18.63	5.8	5.95
Tb	0.43	0.762	0.87	4.21	5.96	3.58	5.31	3.44	0.96	0.954
Dy	3.16	5.83	6.71	24.04	34.12	18.84	31.12	19.39	5.2	5.165
Y	20.17	36.99	54.29	103.3	131.7	71.38	111.2	61.07	28	27.56
Ho	0.736	1.5	1.61	4.76	6.64	3.69	6.04	3.69	1.02	0.998
Yr	2.23	4.64	4.71	12.91	17.49	10.64	15.37	9.38	3	2.95
Tm	0.362	0.79	0.788	1.88	2.59	1.65	2.22	1.39	0.43	0.421
Yb	2.25	4.65	4.78	11.9	15.9	9.78	13.98	9.11	2.6	2.52
Lu	0.344	0.742	0.82	1.99	2.5	1.64	2.16	1.35	0.4	0.403
ΣREE (ppm)	45.97	65.08	91.2	1094	1183	2285	942	515	-	-
$(\Sigma REE/Fe)10^3$	5.05	23.2	1.49	5.5	7.4	11.2	9.91	8.78	-	-
Ce/Ce*	0.98	0.22	0.51	2.55	1.97	7.4	2.04	1.69	-	-
Eu/Eu*	1.21	1.7	1.88	0.93	1.04	0.92	1.08	1.25	-	-
Nd_n/Yb_n	0.3	0.26	0.31	0.83	0.82	0.93	0.81	0.77	-	-
Y/Ho (molar ratio)	50.9	45.7	62.6	40.2	36.8	35.9	34.1	30.6	-	-